



**HAL**  
open science

## Real-time in-situ monitoring of wet thermal oxidation for precise confinement in VCSELs

Guilhem Almuneau, R Bossuyt, P Collière, L Bouscayrol, M Condé, I Suarez,  
V Bardinal, C Fontaine

► **To cite this version:**

Guilhem Almuneau, R Bossuyt, P Collière, L Bouscayrol, M Condé, et al.. Real-time in-situ monitoring of wet thermal oxidation for precise confinement in VCSELs. *Semiconductor Science and Technology*, 2008, 23 (10), pp.105021. 10.1088/0268-1242/23/10/105021 . hal-04828428

**HAL Id: hal-04828428**

**<https://laas.hal.science/hal-04828428v1>**

Submitted on 10 Dec 2024

**HAL** is a multi-disciplinary open access archive for the deposit and dissemination of scientific research documents, whether they are published or not. The documents may come from teaching and research institutions in France or abroad, or from public or private research centers.

L'archive ouverte pluridisciplinaire **HAL**, est destinée au dépôt et à la diffusion de documents scientifiques de niveau recherche, publiés ou non, émanant des établissements d'enseignement et de recherche français ou étrangers, des laboratoires publics ou privés.

# Real-time in-situ monitoring of wet thermal oxidation for precise confinement in VCSELs

**G. Almuneau, R. Bossuyt, P. Collière, L. Bouscayrol, M. Condé, I. Suarez, V. Bardinal and C. Fontaine**

LAAS-CNRS, Université de Toulouse, 7 av. Colonel Roche, 31077 Toulouse, France

E-mail: almuneau@laas.fr

**Abstract.** A new imaging method is presented enabling to monitor the lateral wet thermal oxidation of a thin Al-containing layer embedded in a VCSEL structure. This method is based on the measurement of the modification of the VCSEL reflectivity spectrum inherent to the aperture layer refractive index change, with an observation window restricted to the wavelength ranges for which this reflectivity variation is maximal. The main purpose is the accurate control of the buried confinement aperture, and thereby that of the electro-optical characteristics of the laser device. The kinetics of the lateral oxidation has been studied for small size aperture VCSEL (3-10  $\mu\text{m}$ ) and for long range oxidation depths. This straightforward method based on an optical imaging system will enable to robustly improve production yield of this multifactor dependent technological process.

**PACS :** 42.55.Px Semiconductor lasers; laser diodes, 68.55.-a - Thin film structure and morphology, 78.66.Fd - III-V semiconductors, 81.05.Ea - III-V semiconductors, 78.20.Ci - Optical constants (including refractive index, complex dielectric constant, absorption, reflection and transmission coefficients, emissivity), 81.65.Mq - Oxidation

Submitted to Semiconductor Science and Technology

## 1 Introduction

The wet thermal oxidation of AlGaAs material has led to a very efficient method to realize both electrical and optical confinements in optoelectronic devices. Vertical cavity lasers (VCSEL) have taken benefit from this technology in order to stabilize their performances, and oxide aperture is to date the foremost confinement method used in VCSEL devices [1]. Nevertheless, this technological process suffers from reproducibility, as for the achievements of maximum transverse single-mode power, low threshold currents and high efficiencies are needed as these latter strongly rely on the precise control of the aperture size. Also, the high selectivity of the oxidation reaction regarding the Al composition in the layer implies accuracy much better than 1% in the aimed concentration, which is not routinely attained during the epitaxial growth. The absence of existing techniques for real-time controlling the oxidation process constrains the VCSEL manufacturers to carry out costly repetitive calibrations.

More prospective applications of  $\text{Al}_x\text{O}_y$ -based confinement scheme in non-linear optics [2,3], high quality factor microcavities [4,5], and quantum dot nanodevices for single-photon sources [6] require a high degree of control of the selective oxidation process. For these few examples, the fine tuning of the aperture dimension has a preeminent role on the exploited physical properties.

Several attempts have been reported on the in situ monitoring of the lateral oxide front upon the AlGaAs thermal oxidation. One approach consists in measuring the average change of the VCSEL wafer reflectivity over a large area of patterns during the oxidation process [7]. Besides that this method requires to have uniform replicated patterns on the wafer, signal variations tend to decrease for very small aperture sizes because of the low filling factor. This technique then becomes more difficult to be applied in the case of ultimate sized apertures. The second approach

based on the direct viewing of the oxidizing pattern through a CCD camera is the most straightforward way. This implies the use of an appropriate furnace equipped with a viewport. High reflectivity contrast ( $\Delta R$ ) between oxidized and non-oxidized areas was observed in the case of a fully oxidized Bragg mirror where a large volume of AIAs is converted to low refractive index  $Al_xO_y$  [8], modifying strongly the reflectivity spectrum. The case is much more delicate when the confinement diaphragm size needs to be monitored within VCSELs, that is to say 2 to  $3\mu m$  below its surface. Some critical factors due to the VCSEL structure itself make the observation of the buried  $Al_xO_y$  aperture layer difficult: the small thickness of the buried oxide layer (typically  $< 40$  nm) required for a reduction of optical losses [9], the strong absorption of the top AlGaAs-based mirror stack in the visible spectral range, and the high reflectivity stop-band forbidding any observation within a 70-nm wide window around 850 nm, the operating wavelength.

Fig. 1 shows the difference between calculated reflectivity spectra of non-oxidized and oxidized areas for an 850-nm VCSEL. According to the small effective refractive index change induced by the oxidation of the thin 25-nm  $Al_{0.98}GaAs$  aperture layer, the difference is only slight. We can note that, contrary to a fully oxidized AIAs/GaAs Bragg mirror [8], the general shape of the reflectivity spectrum remains almost the same after oxidation in the case of a VCSEL. Indeed, monitoring the aperture in a standard VCSEL structure cannot be simply done by the use of a high pass filter, but requires a specific method enabling the detection of the minor changes of the reflectivity side-lobes. This fact is sustained by the reduction of exploitable information when the signal is integrated across a large wavelength range due to the balance between negative and positive contrast contributions.

We present in Fig. 2 several examples of images taken at  $25^\circ C$  under illumination at different

narrow filtered wavelength windows, depicting different cases of observable and non-observable oxide in the VCSEL structure. We show two examples of negative and positive contrasted images respectively at 755 nm and 907 nm, and two examples with no observable oxide at 835nm (within the VCSEL reflectivity stop-band), and 967 nm. The oxide layer can be easily detected for each wavelength presenting a more distinct contrast amplitude around the negative/positive amplitude maxima of the  $\Delta R$  curve.

We have applied this spectral technique to control oxide formation carried out at high temperature. At the standard process temperatures (400-450°C), the reflectivity spectra are changed due to the temperature dependence of the refractive indices (as seen in fig. 1) of the different materials [10]. Moreover, the thermal red-shift of the absorption for AlGaAs layers, present in the top Bragg mirror, allows us to observe large  $\Delta R$  only in the high wavelength region (>900nm). As at room temperature, the reflectivity difference  $\Delta R$  is found to be more important for some wavelengths (fig. 1). Since  $\Delta R$  is now hardly detectable around the VCSEL emitting wavelength [11], we propose to improve the sensitivity of the measurement has been by probing around sidelobes for which  $\Delta R$  is most significant.

## **2 Experimental setup**

All our experiments have been carried out on standard 850nm VCSEL structures. An  $\text{Al}_{0.98}\text{Ga}_{0.02}\text{As}$  layer (25 nm) – to be oxidized – is positioned just above the cavity, and overlaid by a 26-periods output Bragg mirror (DBR). Beforehand the thermal oxidation process, mesas have been formed by reactive ion etching (ICP-RIE), and the sidewalls deoxidized in an  $\text{HCl}:\text{H}_2\text{O}$  (1:10) solution.

The thermal wet oxidations were realized in a small quartz cylindrical oven equipped with a heater enabling process temperatures in the 300-500°C range. The heater temperature is

controlled with a thermocouple, and the wafer temperature calibrated with a low temperature infrared pyrometer. The oxidizing gas stream was produced by flowing dinitrogen through a water-filled bubbler heated at 95°C. The geometry of this oven allows us to observe the surface of the processed sample at a scale of a 30  $\mu\text{m}$ -diameter mesa using an optical microscope equipped with a near infrared sensitive CCD camera. This makes it possible to acquire images of the VCSEL mesa during the oxidation. The illumination of the microscope was modified in order to filter a tunable narrow band ( $\Delta\lambda \approx 20 \text{ nm}$ ) of the white light spectrum thanks to a 1/8 meter monochromator. Narrower source bandwidth could be chosen in order to improve the wavelength selectivity and thus the sensitivity of the measurement, but the integrated intensity would be then too low for the CCD acquisition in our configuration.

Then observation of the VCSEL mesa being laterally oxidized is achieved just by selecting the adequate wavelength for which  $\Delta R$  between oxidized and non-oxidized zones is enhanced (cf. fig. 1).

### **3 Monitoring of the oxide aperture**

The video frames taken during the oxidation process with a filtered illumination at around 935 nm are given in fig. 4. Four different mesa types have been observed during the oxidation at 420 °C: three circular ones (31, 33 and 35  $\mu\text{m}$ ) and a 41  $\mu\text{m}$  wide rectangle. The evolutions of the oxide aperture show a linear progression of with a mean oxidation rate of 1.6  $\mu\text{m}/\text{min}$ . We have measured the standard deviation of our oxide aperture diameter measurement in the range of  $\pm 0.5\text{-}0.6 \mu\text{m}$ , which corresponds to the limitation of the pixel size of our CCD camera. This results is comparable to or slightly better than the best resolution achieved to date without *in-situ* control ; nevertheless a significant improvement is brought by the facts that no preliminary calibration is required, and that the spatial resolution only rely on the performances of the image

acquisition chain (microscope, CCD sensor, image processing). The aperture decrease is shown in fig. 5 for the three circular mesas (31, 33 and 35  $\mu\text{m}$ ). The corresponding plot of experimental data from the monitoring sequence presented in fig. 4 is presented in fig. 5.

We observe a linear behavior of the oxidation width *vs.* time in the range of aperture diameters from 15  $\mu\text{m}$  down to 3  $\mu\text{m}$ . The oxide progression rate is similar for the three different mesas, without any observable change in particular in the low aperture diameters ( $< 5 \mu\text{m}$ ).

This *in-situ* monitoring method, easily implementable, is especially promising for realizing repetitively optimized aperture sizes for transverse single-mode operation of ridge laser and VCSEL devices.

#### **4 Conclusions**

A direct observation method has been proposed for the monitoring of the selective thermal wet oxidation of a high Al-content AlGaAs layer embedded in VCSEL structures, with an oxide thickness as small as 25 nm. In particular, this technique enables to control accurately the aperture diaphragm size, and accordingly the performances of the devices. Formation of apertures with diameters down to 3  $\mu\text{m}$  can be real-time controlled independently of the initial mesa dimensions and the  $\text{Al}_x\text{Ga}_{1-x}\text{As}$  alloy composition, the final resolution depending only on the characteristics of the optical microscope and CCD camera sensor used. Furthermore, we have demonstrated that oxidation kinetics can be directly and rapidly acquired, opening to a thorough understanding of the different mechanisms involved in selective oxidation of high Al content layers embedded in III-V semiconductor structures.

#### **Acknowledgments**

G.A. and R. B would like to thank Prof G. Otrio for fruitful discussions throughout this project.

The authors wish to acknowledge the French National Research Agency (ANR) for funding this work through the "Jeunes Chercheurs" research program (Project ANR-06-JCJC-0029).



## Figures

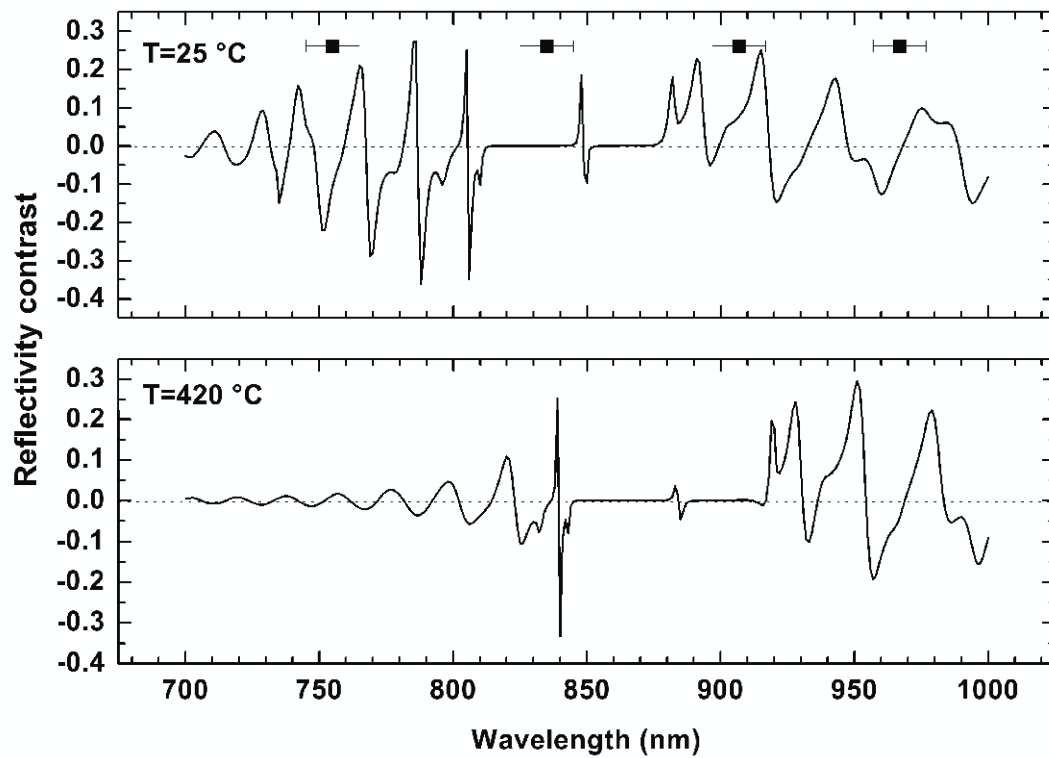


**Figure 1.** Difference in the top-reflectivity of non-oxidized and oxidized areas of an 850nm-VCSEL at room temperature (25°C) and at the process temperature (420°C). Marked wavelength ranges correspond to the observed images presented in Fig. 2.

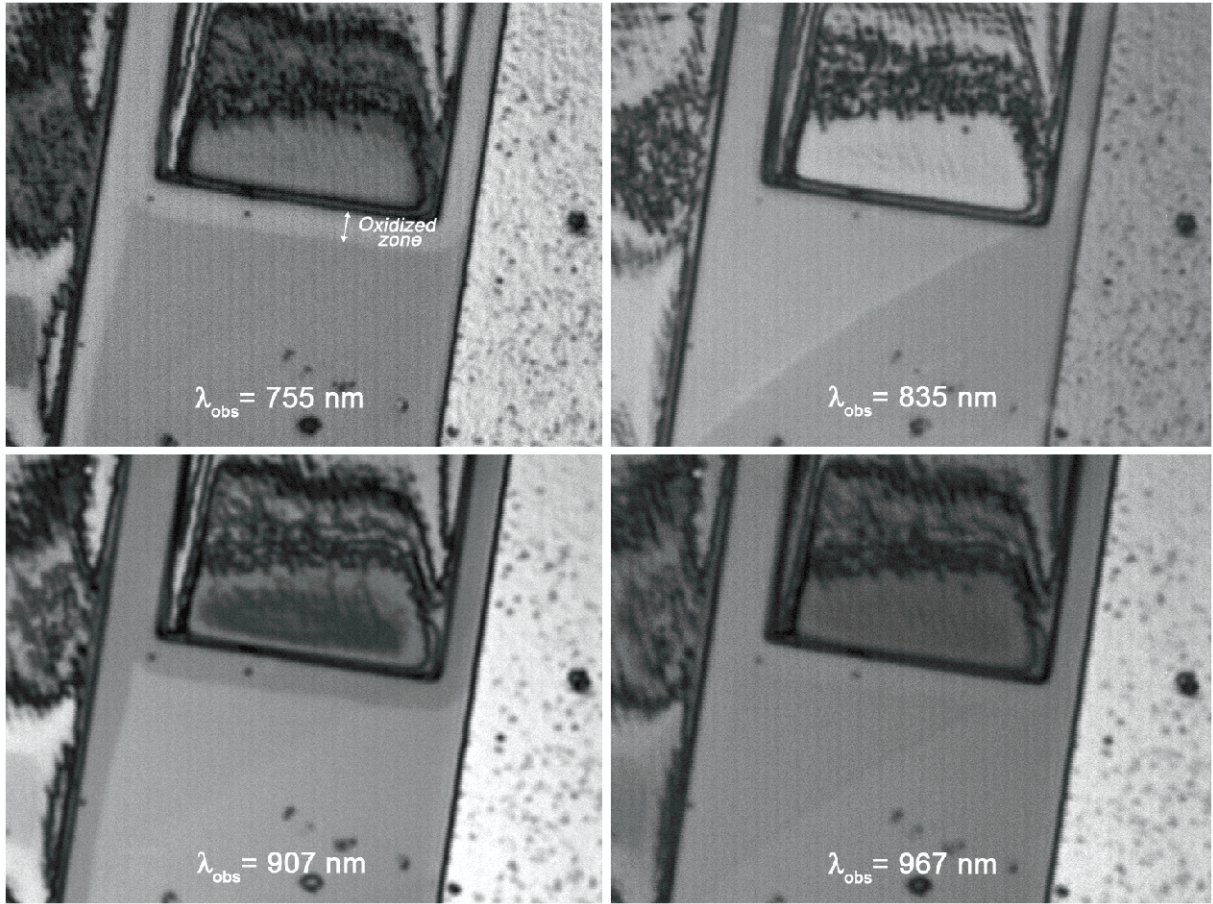


**Figure 2.** Different contrasted images of a partially oxidized 850-nm-VCSEL structure illuminated with four different wavelengths at 25°C.

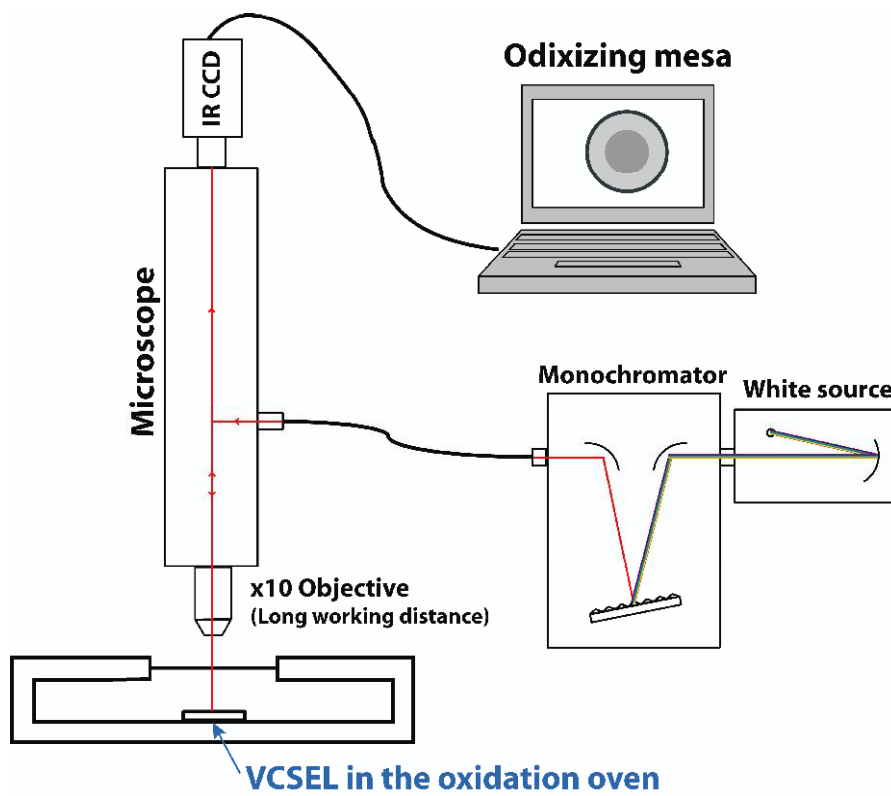
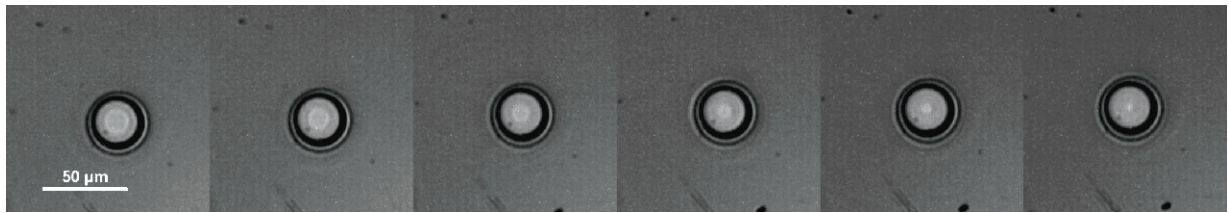
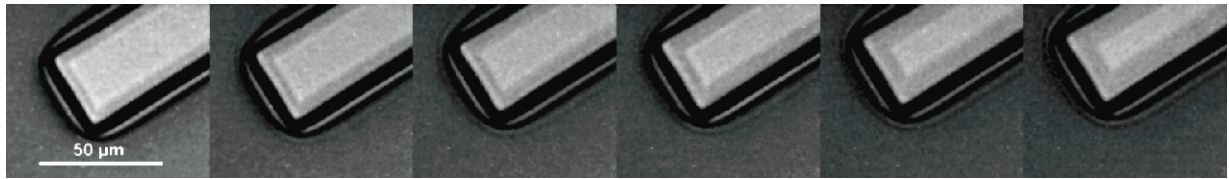


**Figure 3** Experimental optical setup for the *in-situ* thermal oxidation monitoring



(a)



(b)

**Figure 4** Real-time observation of buried lateral thermal oxidation in 850 nm-VCSEL, in the case of a circular mesa (a), and a rectangular one (b). The time interval between subsequent snapshots is 1'30".

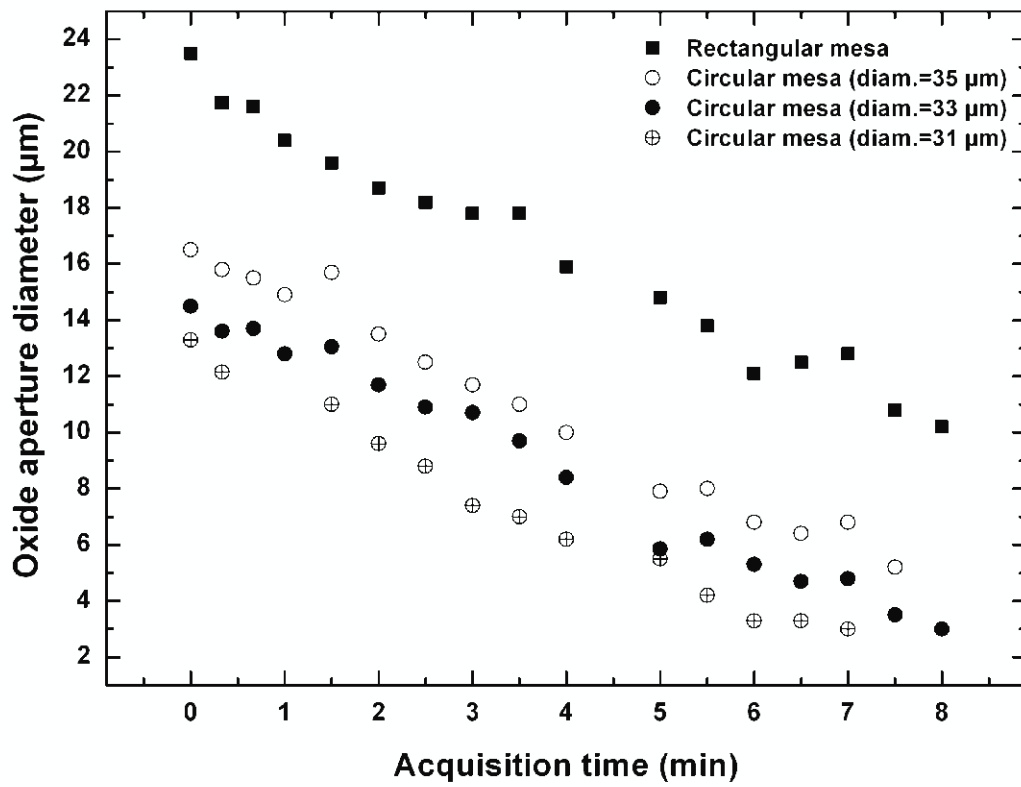


**Figure 5** Oxide aperture variation during the monitoring for a rectangular (width=41 $\mu\text{m}$ ) and three different circular mesas (diameters = 31, 33 and 35 $\mu\text{m}$ ). The time scale origin starts at the beginning of the observation, and not when the oxidation process starts.

## References

- [1] Wiedenmann D , Grabherr M, Jäger R, and King R 2006 High volume production of single-mode VCSELs *Proc. of the SPIE* **6132** 1-12
- [2] Fiore A , Berger V, Rosencher E, Bravetti P, and Nagle J 1998 Phase matching using an isotropic nonlinear optical material *Nature* **391** 463-466
- [3] Scaccabarozzi L, Fejer M M, Huo Y, Fan S, Yu X, and Harris J S 2006 Enhanced second-harmonic generation in AlGaAs/Al<sub>x</sub>O<sub>y</sub> tightly confining waveguides and resonant cavities *Optics Lett.* **31** 3626-3628
- [4] Stoltz N G, Rakher M, Strauf S, Badolato A, Lofgreen D D, Petroff P M, Coldren L A and Bouwmeester D 2005 High-quality factor optical microcavities using oxide apertured micropillars *Appl. Phys. Lett.* **87** 031105
- [5] Shin J H, Han I Y and Lee Y H 1998 Very small oxide-confined vertical microcavity lasers with high-contrast AlGaAs–Al<sub>x</sub>O<sub>y</sub> mirrors *IEEE Photon. Technol. Lett.* **10** 754-756
- [6] Monat C, Alloing B, Zinoni C, Li L H and Fiore A 2006 Nanostructured current-confined single quantum dot light-emitting diode at 1300 nm *Nano Lett.* **6** 1464
- [7] Sakamoto A, Nakayama H and Nakamura T 2002 Fabrication control during AlAs oxidation of the VCSELs via optical probing technique of AlAs lateral oxidation (OPTALO) *Proc. SPIE* **4649** 211-217
- [8] Feld S A, Loehr J P, Sherriff R E, Wiemer J and Kaspi R 1998 In situ optical monitoring of AlAs wet oxidation using a novel low-temperature low-pressure steam furnace design *IEEE Photon. Technol. Lett.* **10** 197-199

- [9] Demeulenaere B, Bienstman P, Dhoedt B and Baets R G 1999 Detailed study of AlAs-oxidized apertures in VCSEL cavities for optimized modal performance *IEEE J. Quantum Electron.* **35** 358-367
- [10] Bardinal V, Legros R and Fontaine C 1995 In situ measurement of AlAs and GaAs refractive index dispersion at epitaxial growth temperature *Appl. Phys. Lett.* **67** 244
- [11] Bardinal V, Averseng L, Bringer C, Camps T, Polesel-Maris J, Dubreuil P, Fontaine C, Bedel-Pereira E, Vergnenègre C and Muñoz-Yagüe A Experimental demonstration of oxide modes influence in a dual-purpose oxide-confined vertical-cavity surface-emitting laser *Appl. Phys. Lett.* **81** 1771-2

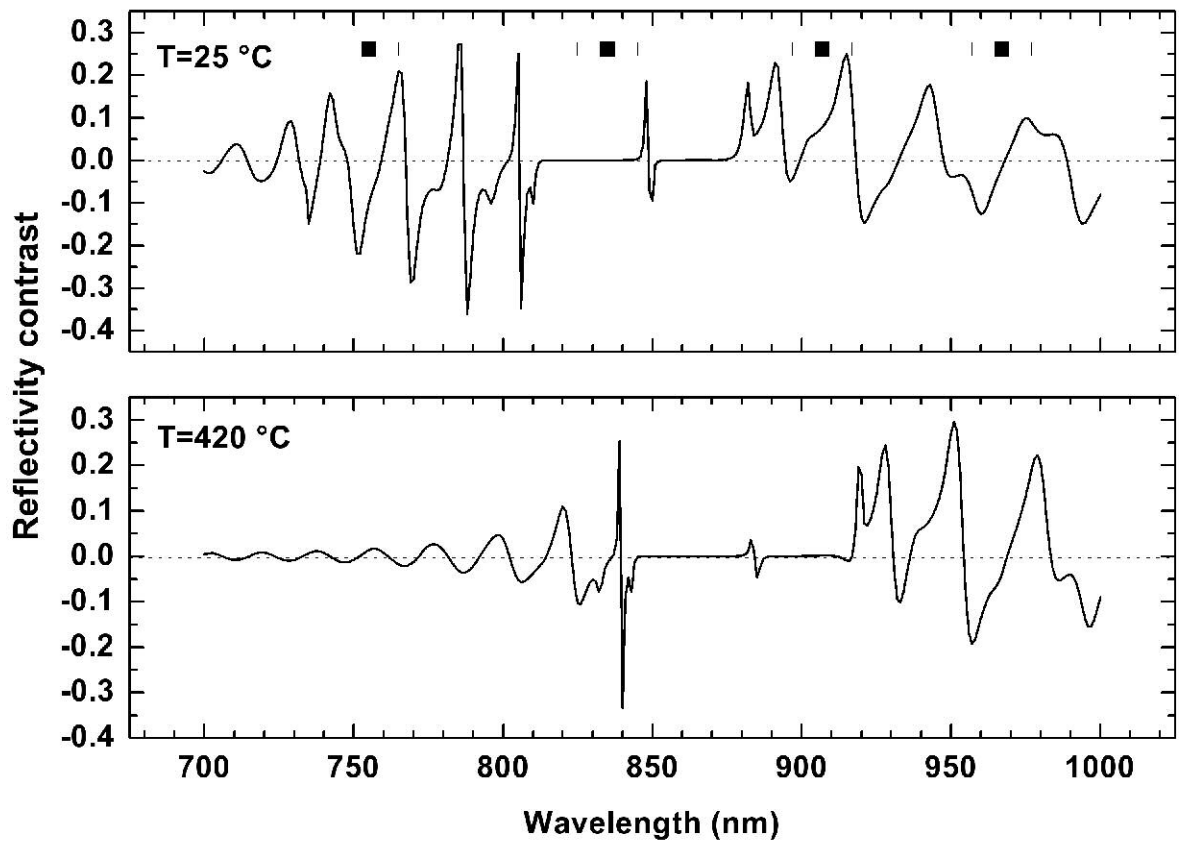
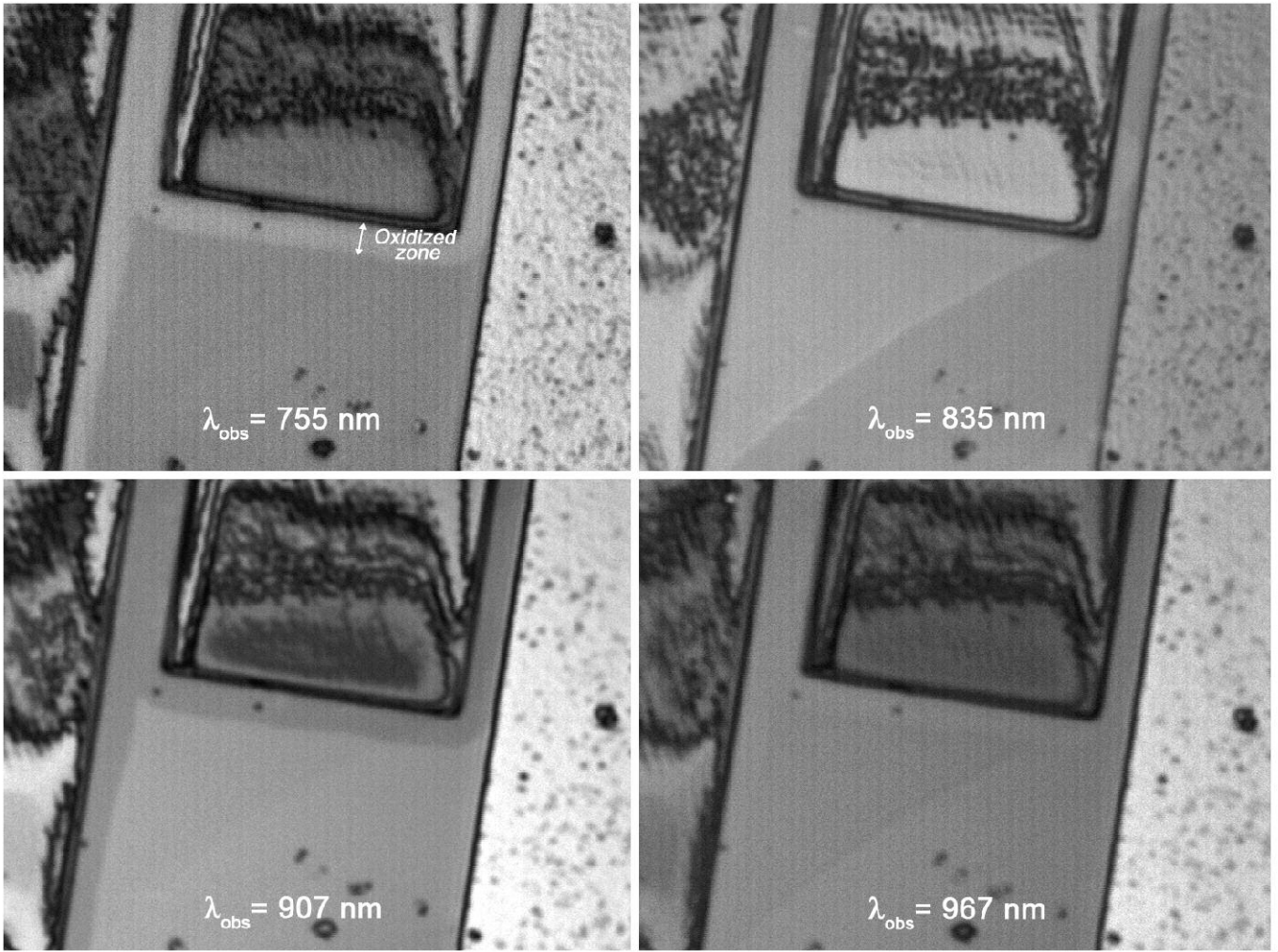


Figure 1 (Almuneau\_fig1.tif)





**Figure 2 (Almuneau\_fig2.bmp)**

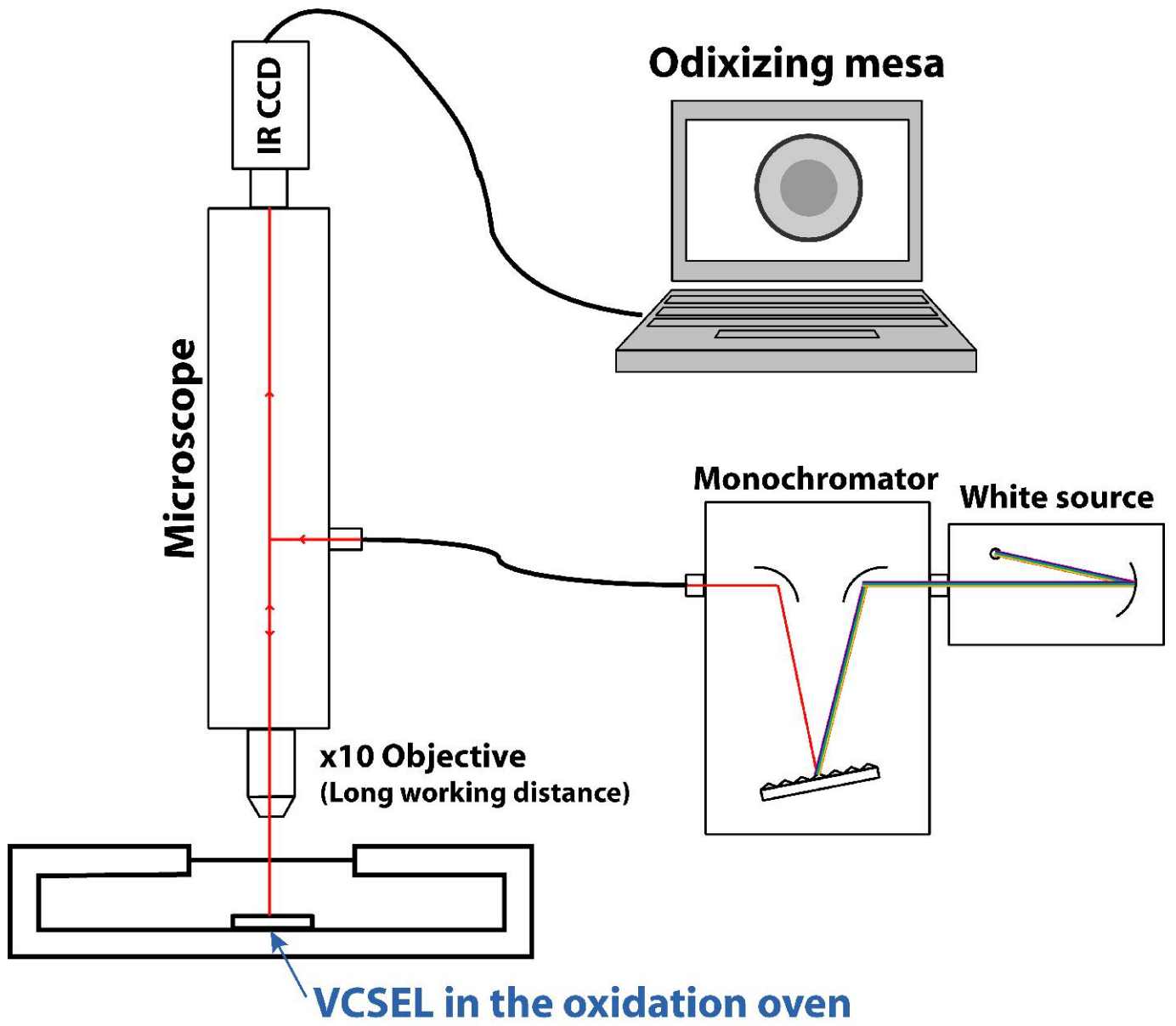
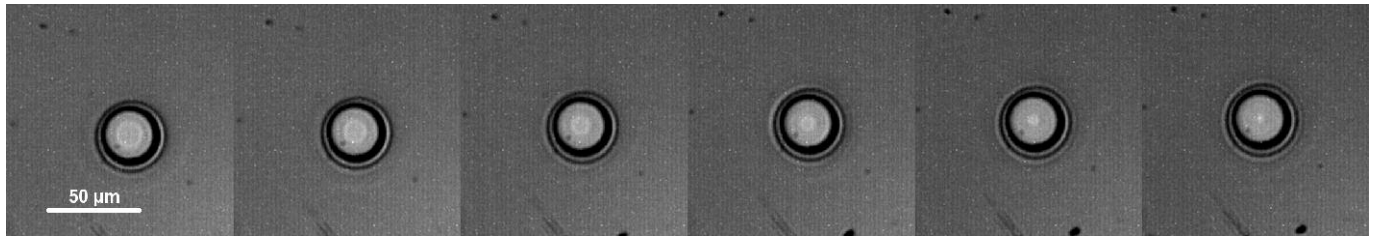
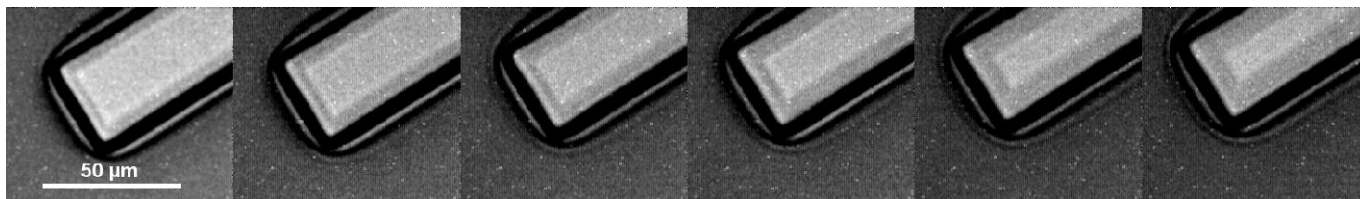


Figure 3 (Almuneau\_fig3.tif)



**Figure 4 (Almuneau\_fig4a\_R1.bmp)**



**Figure 5 (Almuneau\_fig4b\_R1.bmp)**

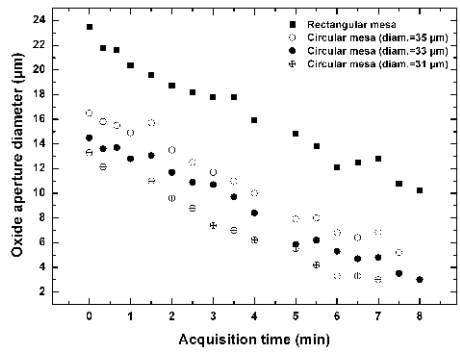


Figure 6 (Almuneau\_fig5\_R1.bmp)